Article

Journal of Industrial Textiles

2020, Vol. 49(7) 943–966

DOI: 10.1177/1528083718801359
journals.sagepub.com/home/jit
SAGE

Structure–property relationship and controlled drug release from multiphasic electrospun carvacrol-embedded polylactic acid/polyethylene glycol and polylactic acid/polyethylene oxide nanofiber mats

Roberto Scaffaro, Fortunato Emmanuel Gulino and Francesco Lopresti

Abstract

Electrospinning technologies gained considerable interest over the last decade. In this study, it is proposed a systematic study of polylactic acid/polyethylene glycol (PLA/PEG) and polylactic acid/polyethylene oxide (PLA/PEO) electrospun blends at different concentrations. The effect of blend composition and PEG molecular weight on the morphological and mechanical properties of the mats was evaluated. Furthermore, the kinetic release of carvacrol as model drug in phosphate buffer saline at 37°C was studied and the data were then fitted using an exponential model. The scanning electron microscopy revealed that the morphology of the mats was strongly dependent on the relative ratio PLA:PEG, PLA:PEO and in the presence of carvacrol. Furthermore, the mechanical properties of the mats as well as their carvacrol release rate were successfully tuned by changing the relative ratio of the blend components.

Dipartimento di Ingegneria Civile Ambientale Aerospaziale dei Materiali, Universita degli Studi di Palermo, Palermo, Italy

Corresponding author:
Roberto Scaffaro, Dipartimento di Ingegneria Civile Ambientale Aerospaziale dei Materiali, Viale delle Scienze, Universita degli Studi di Palermo, Ed. 6., Palermo 90128, Italy.
Email: roberto.scaffaro@unipa.it

Keywords
Chemistry, diffusion, fabrication, materials, medical textiles, nonwoven, processing, strength, structure properties

Introduction

Electrospinning is an emerging processing technique that allows fabricating nonwoven mats composed of continuous fibers exhibiting diameters ranging from micro- to nano-meters [1–5]. The increasing interest in electrospun micro/nanofibrous membranes is due to their high porosity, specific surface, as well as due to tunable mechanical properties and topological features [6–13].

Over the last few years, several approaches were proposed in order to enhance the properties of electrospun mats such as the use of nanofillers [2,14,15], surface functionalization [16], and/or the use of appropriate polymer blends [17–26].

In particular, there are many scientific papers that propose blending of different polymers to improve mechanical performances [17–19], hydrophilicity [20,21], or biocompatibility [22–25].

Among the several synthetic polymers used for electrospinning, polyvinyl alcohol [27,28], polyglycolic acid [29], poly-ε-caprolactone [2,19,30–32], and polylactic acid (PLA) were often investigated as main matrix for the fabrication of electrospun fibers, for tissue engineering and for drug delivery applications [16,33–35]. PLA is a semicrystalline thermoplastic polymer exhibiting a fragile behavior, with relative high elastic modulus and low elongation at break [36–44]. In several scientific papers, PLA was blended with polymers obtained from the polymerization of ethylene oxide usually indicated either as polyethylene glycol (PEG) if $Mw < 20{,}000$ Da or polyethylene oxide (PEO) if $Mw > 20{,}000$ Da. These blends were found to improve both the biocompatibility and the biodegradability and were also found to increase the hydrophilicity, the ductility, and the melt processability of PLA [39,44–46]. PEG is an hydrosoluble polymer partially miscible in PLA whose molecular weight can affect both the miscibility and the release rate of incorporated drugs [47,48]. This is a crucial feature since drug-containing electrospun membranes are deeply investigated for biomedical application and several studies revealed that the effectiveness of the antimicrobial activity over time is mainly determined by the release rate of the antimicrobial agents [49–52]. Kuang et al. successfully prepared a PLA-based material for local cancer treatment exhibiting a biphasic release kinetics by tuning the weight ratio of PEO and PLA in blends [46]. Sirc et al. used PEG at different molecular weight (6000 20,000 and 35,000 Da) as additives to modify the immunosuppressant cyclosporine A release kinetics from PLA electrospun membranes [53].

In this context, carvacrol (CRV) is one of the most studied phenolic essential oils investigated as antimicrobial agent for PLA-based materials. The scientific interest on this compound considerably strengthened because of its broad spectrum of biological and pharmacological properties such as: (i) anti-inflammatory, (ii) antimicrobial, (iii) antioxidant, (iv) antitumor, and (v) antimutagenic activities [54,55].

In our previous works, we evaluated the processing parameters and the effect of CRV content on the structure, property relationships, and on the release kinetics of electrospun PLA/CRV membranes [54]. To the best of our knowledge, this work proposes for the first time a systematic study of PLA/PEG and PLA/PEO electrospun blends at different concentrations in order to evaluate the effect of blend composition and PEG molecular weight on morphological, mechanical, and wettability properties of the mats. Furthermore, in order to put into evidence the influence of PEG and PEO on the release kinetic of a model drug loaded into PLA, CRV was filled in the nanofibers at 28 wt% with respect to the polymer phase, and the kinetic release in phosphate buffer saline (PBS) at 37°C was fitted with an exponential model.

Experimental section

Materials and methods

PLA 2002D (Mw 215,000 Da; D-lactide content 4%) [56] was purchased from NatureWorks. PEG (Mw 10,000 Da), PEO (Mw 100,000 Da), CRV, acetone (Ac), chloroform (TCM), and PBS were purchased from Sigma Aldrich. All the reactants were of ACS grade (purity > 99%). PLA was vacuum dried overnight at 90°C while the other components were used as received.

The 10 wt% of PLA/PEG or PLA/PEO at different relative ratio were added to 20 ml of TCM:Ac (2:1 vol), and completely dissolved by stirring overnight to obtain a homogeneous solution. The relative compositions of the blends here produced are listed in Table 1.

In order to prepare CRV-containing membranes, CRV was added to the polymeric solutions at 28 wt.% with respect to polymer phase according to the results of a previous paper [30].

The preparation of the membranes was performed by a conventional electrospinning equipment (Linari Engineering-Biomedical Division, Italy). The polymeric solutions were filled in 10-ml glass syringe equipped with a 19G stainless steel needle. The process was performed using the following parameters: flow rate, 2 ml/h; supplied high voltage, 15 kV; distance between needle tip and collector, 15 cm; temperature, 25°C; and relative humidity, 40%. The nanofibers were collected on a grounded collector wrapped in an aluminum foil. The process was performed for 30 min in order to obtain membranes approximately 25 μm thick. The collected membranes were subsequently dried overnight under fume hood in order to remove any residual solvent.

Morphological analysis

The morphology of the nanofibers was observed by using a scanning electron microscopy (Phenom ProX, Phenom-World, The Netherlands). The samples were positioned on an aluminum stub using an adhesive carbon tape and then

Table 1. Composition of the PLA/PEG and PLA/PEO blends.

Sample code	PLA (%)	PEG (%)	PEO (%)
PLA	100	0	0
25% PEG	75	25	0
50% PEG	50	50	0
75% PEG	25	75	0
PEG	0	100	0
25% PEO	75	0	25
50% PEO	50	0	50
75% PEO	25	0	75
PEO	0	0	100

PEG: polyethylene glycol; PEO: polyethylene oxide; PLA: polylactic acid.

sputter coated with gold (Sputtering Scancoat Six, Edwards) for 90 s under argon atmosphere before imaging to avoid electrostatic discharge during the test.

FT-IR/ATR analysis

The chemical surface properties of the samples were assessed by FT-IR/ATR analysis carried out by using a Perkin-Elmer FT-IR/NIR Spectrum 400 spectrophotometer. The spectra were recorded in the range 4000–400 cm^{-1}.

Mechanical properties

Tensile mechanical measurements were carried out with a laboratory dynamometer (Instron model 3365, UK) equipped with a 1 kN load cell. The tests were performed on rectangular shaped specimens (10×90 mm) cut off from the mats. The measurements were performed by using a double crosshead speed: 1 mm min^{-1} for 2 min and 50 mm min^{-1} until fracture occurred because of the high elongation of the sample here investigated. The grip distance was 20 mm, whereas the sample thickness was measured before each measurement.

Seven samples were tested for each material and the average values of the mechanical parameters and standard deviations were reported. The representative nominal stress–strain curves were reported for each material as well as their elastic modulus (E), tensile strength (TS), and elongation (ε).

Complex viscosity determination

Rheological characterizations were performed on the polymeric solutions using a rotational rheometer (Mars, Thermofisher). A 25-mm parallel-plate geometry

was used and all tests were performed at 25°C. Oscillatory frequency sweep tests were performed at a constant stress of 1 Pa with an increase of angular frequency from 1 to 100 rad/s.

Kinetics of release of the essential oil constituents from the polymeric films

A series of CRV/PBS solutions containing 1 to 50 mg/l were analyzed by using UV/vis spectrophotometer (model UVPC 2401, Shimadzu Italia s.r.l., Milan, Italy) in order to obtain a calibration curve correlating the absorbance peak intensity of CRV to its concentration in PBS. In the concentration range here investigated, the calibration curve was found to be a line. The maximum absorbance peak of CRV was detected at 272 nm. The release of the essential oils from the films was investigated by immersing a preweighed sample (a rectangular of 10×40 mm) in 10 ml of PBS at 37°C. The absorbance peak intensity of the storage solutions was measured at specific time intervals and converted to the quantities of essential oil released through the calibration line. All the samples were immersed in 10 ml of fresh PBS after each measurement. We therefore reported the cumulative oil release calculated by sequentially adding the oil released after each step. Each measurement was performed in triplicate.

Wettability determination

Static contact angles were measured on all the samples using deionized water as a fluid by an FTA 1000 (First Ten Ångstroms, UK) instrument. More in detail, 4 μL of deionized water were dropped onto fiber mats. Images of the water droplet were taken at a time of 10 s. At least seven spots of each composite nanofiber mat were tested and the average value was taken.

Statistical analysis

Statistical analyses of the data were performed through ANOVA by using the GraphPad Prism version 6 software (GraphPad Software Inc., La Jolla, CA). Significant differences among mean values, where applicable, were determined by the means of ANOVA and by Tukey's HSD post hoc test for multiple comparisons. In all cases, a value of $p < 0.05$ was considered statistically significant.

Results and discussion

Morphology, ATR-FTIR, and wettability of electrospun PLA/PEG and PLA/PEO blends

SEM micrographs of electrospun materials are shown in Figure 1 while in Figure 2 the mean diameter of the electrospun fibers as a function of PEG and PEO amount is reported.

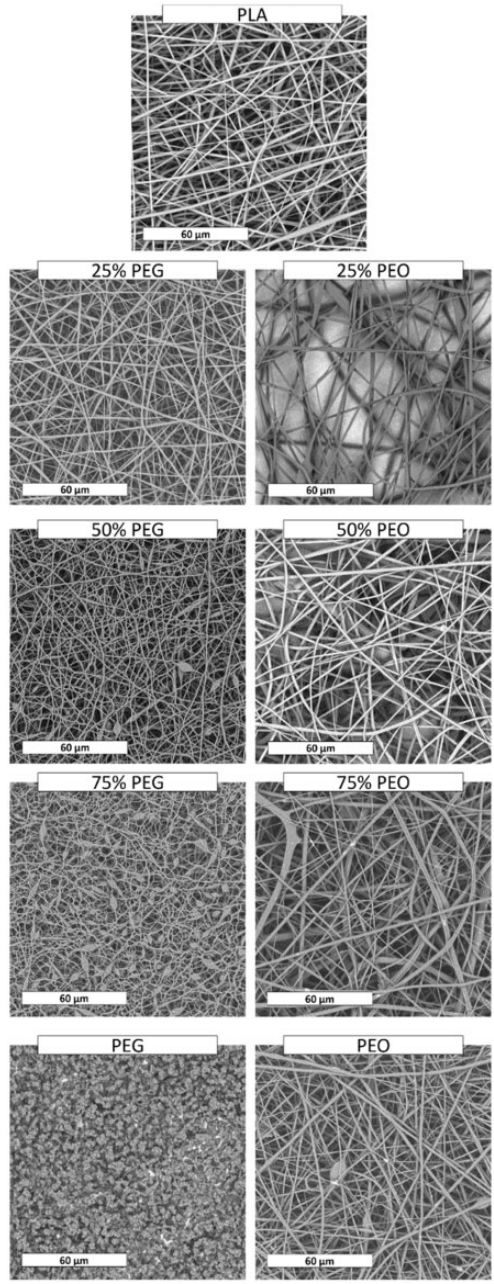

Figure 1. SEM micrographs of electrospun blends. PEG: polyethylene glycol; PEO: polyethylene oxide; PLA: polylactic acid.

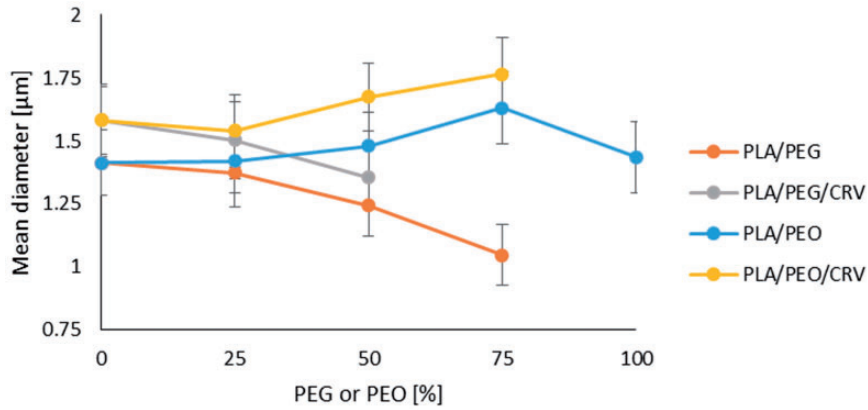

Figure 2. Mean diameter of the electrospun fibers as a function of the amount of PEG and PEO loaded with 28 wt% of CRV or in the absence of CRV. CRV: carvacrol; PEG: polyethylene glycol; PEO: polyethylene oxide; PLA: polylactic acid.

The micrographs reveal that the fibres are randomly oriented and their diameters are in the microscale range for all the investigated systems. In particular, for PLA it is possible to observe that the fibres present homogeneous diameters all over the surface and smooth and regular morphology. The fibers of the blends mats are less regular if compared with those of neat PLA electrospun mats, in particular at higher PEG and PEO composition. They also present different mean fibers diameter as shown in Figure 2.

More in detail, blends containing 25 wt% of PEG (25% PEG) exhibit fibers morphology and mean diameter (1.38 ± 0.27 µm) very similar to that of neat electrospun PLA (1.41 ± 0.26 µm). On the other hand, the fibers mean diameter decreases upon increasing PEG amount (1.24 ± 0.24 µm for 50% PEG and 1.05 ± 0.23 µm for 75% PEG) becoming statistically different ($p < 0.05$) if compared to neat PLA. Furthermore, for the systems containing 50 wt% and 75 wt% of PEG (50% PEG and 75% PEG), the fibers show a certain number of beads, very numerous for the 75% PEG mats. Furthermore, SEM analysis revealed that neat PEG cannot be electrospun with the chosen processing parameters resulting in the formation of micrometric particles. This phenomenon agrees with other scientific works revealing that polymers with molecular weight below 50,000 Da are hardly electrospinnable [57].

Figure 2 highlights that the presence of 25 wt% and 50 wt% of PEO (25% PEO and 50% PEO) induces a slight increase of fibers diameter (1.42 ± 0.12 µm and 1.48 ± 0.13 µm, respectively) when compared to those of neat electrospun PLA (1.41 ± 0.13 µm). The 75% PEO system shows very irregular fibers and a very heterogeneous fibers distribution with mean fibers diameter (1.632 ± 0.145 µm) statistically different ($p < 0.05$) when compared to neat PLA. Neat PEO exhibits quite regular fibers presenting mean diameter very similar to that of PLA (1.44 ± 0.14 µm).

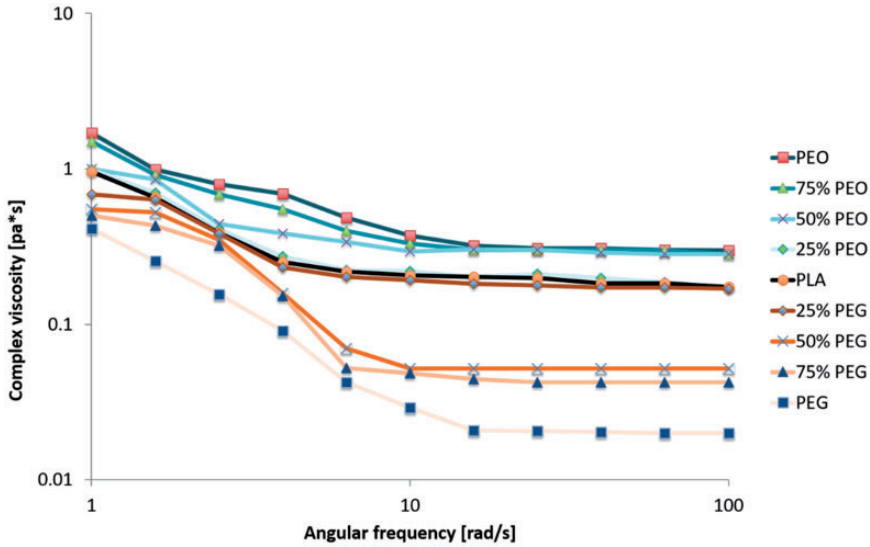

Figure 3. Complex viscosity of the polymeric solutions. PEG: polyethylene glycol; PEO: polyethylene oxide.

Generally, it is well known that an increase of the solution viscosity induces the formation of fibers with larger average diameters [2,58]. The correlation between the viscosity of the solutions and the fibers diameter of electrospun mats was investigated by studying the complex viscosity of the polymeric solution as reported in Figure 3.

As expected, and coherently with the morphological observation, PLA/PEO solutions show higher viscosity if compared to neat PLA solution in the whole range of frequencies and it increases upon increasing PEO content.

On the other hand, the rheological tests reveal that the viscosities of all the materials containing PEG are lower than the viscosity exhibited by the pure matrix and, in agreement with SEM analysis, they decrease upon increasing the PEG content.

Figure 4 shows the morphology of CRV-loaded electrospun polymer blends as a function of PEG and PEO amount. Adding 28 wt% of CRV in PLA induces a worsening of the fibers morphology.

In fact, from SEM analysis shown in Figure 4, it is possible to observe that the morphology of PLA/CRV fibers is a little bit rougher when compared to neat electrospun PLA (Figure 1) and that the fiber's diameter distribution is more heterogeneous with a slight increase of the mean diameter size (Figure 2). In Figure 4, 75% PEG/CRV and PEG/CRV are not shown since there was no deposition of material on the collector with the chosen processing parameters.

The 25% PEG/CRV show quite smooth and regular fibers characterized by thinner diameter when compared to 25% PEG. A different behavior was observed

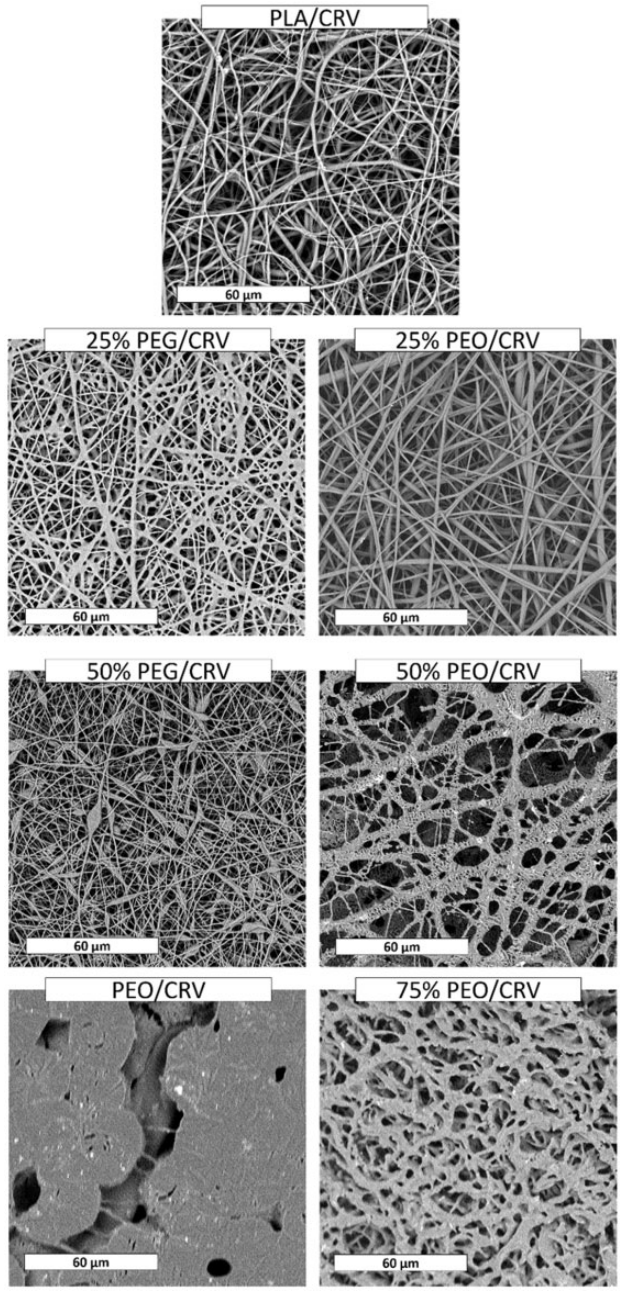

Figure 4. SEM micrographs of electrospun blends loaded with 28 wt% of CRV. CRV: carvacrol; PEG: polyethylene glycol; PEO: polyethylene oxide; PLA: polylactic acid.

for 50% PEG/CRV that shows a higher number of beads among the fibers when compared to the equivalent system without CRV.

The addition of CRV in 25% PEO mats (25% PEO/CRV) did not significantly affect the fiber's morphology. In fact, their fibers are similar to that of the corresponding blend without CRV. On the other hand, upon increasing the PEO amount, the morphologies are evidently different, with a higher amount of merged fibers. SEM images of PEO/CRV showed a quite compact morphology with sporadic short fibers.

These analyses revealed that CRV did not significantly modified blend morphology at higher PLA content. At the same time, the morphology was found to be worsened at the other composition.

Figure 5(a,b) shows ATR-FTIR measurements carried out on neat PLA and on all PLA/PEG (Figure 5(a)) and PLA/PEO (Figure 5(b)) mats. As listed in Table 2, the bands at 1360 and 1344 cm^{-1} of PEO and PEG are assigned to CH_2 wagging modes; the –C–O– stretching vibrations of PEG and PEO can be related to three bands at 1148, 1113 and 1061 cm^{-1}. The CH_2 rocking band of crystalline PEG occurs at 962 cm^{-1} [59].

The ATR-FTIR spectra of electrospun PLA revealed a clear band at 1211 cm^{-1} (–C = O bend) whereas a faint band is evident around 1265 cm^{-1} (–C–O– stretch) which is typical of PLA (Table 2).

As expected, the FTIR-ATR spectrum of PLA/PEG and PLA/PEO blends show bands that are typical of both PLA and PEG or PEO. In particular, at 1344 cm^{-1} (CH_2 of PEG and PEO, band 15 in Figure 5(a,b)) it is possible to observe a band with increasing intensity upon increasing the PEG or PEO amount in the blends. On the other hand, the band related to the –C = O carbonyl stretch of PLA at 1747 cm^{-1} (band 1 in Figure 5(a)) proportionally decreases upon increasing PEG or PEO amount. The results highlight that there is no evidence about chemical interaction between polymers in blending systems.

CRV shows characteristic bands at 2960 (–CH– stretching), 1459, 1382 and 1346 (CH deformation), and 866 and 812 cm^{-1} (aromatic ring) [61]. In Figure 4(a) and (b) it is possible to observe that all the blends loaded with CRV show several bands ascribable to the essential oil. In particular, for all the ternary systems, the band at 812 cm^{-1} can be observed, related to the CRV aromatic ring thus confirming the successful inclusion of additive in the electrospun nanofibers.

It is well known that PEG and PEO modify the wettability of PLA [46]. Electrospun PLA/PEG and PLA/PEO blends, loaded with 28 wt% of CRV or in the absence of CRV, were characterized with water contact angle (WCA) in order to verify the hydrophilicity of the systems. Electrospun PLA, as already observed in other works [62], showed a θ_w of $115.4° \pm 1.2°$ while PLA/CRV mats show a θ_w of $85.9° \pm 0.8°$. All the PLA/PEG and PLA/PEG/CRV blends display a θ_w of 0°. The same was observed for the PLA/PEO systems while PLA/PEO/CRV blends show an increasing value of θ_w upon increasing the PEO content. In particular θ_w of 25% PEO/CRV is 0°, θ_w of 50% PEO/CRV is $35.3° \pm 0.6°$, the 75% PEO/CRV shows a θ_w of $41.8° \pm 0.7°$ and for PEO/CRV θ_w is $58.4° \pm 0.7°$. The wettability of the

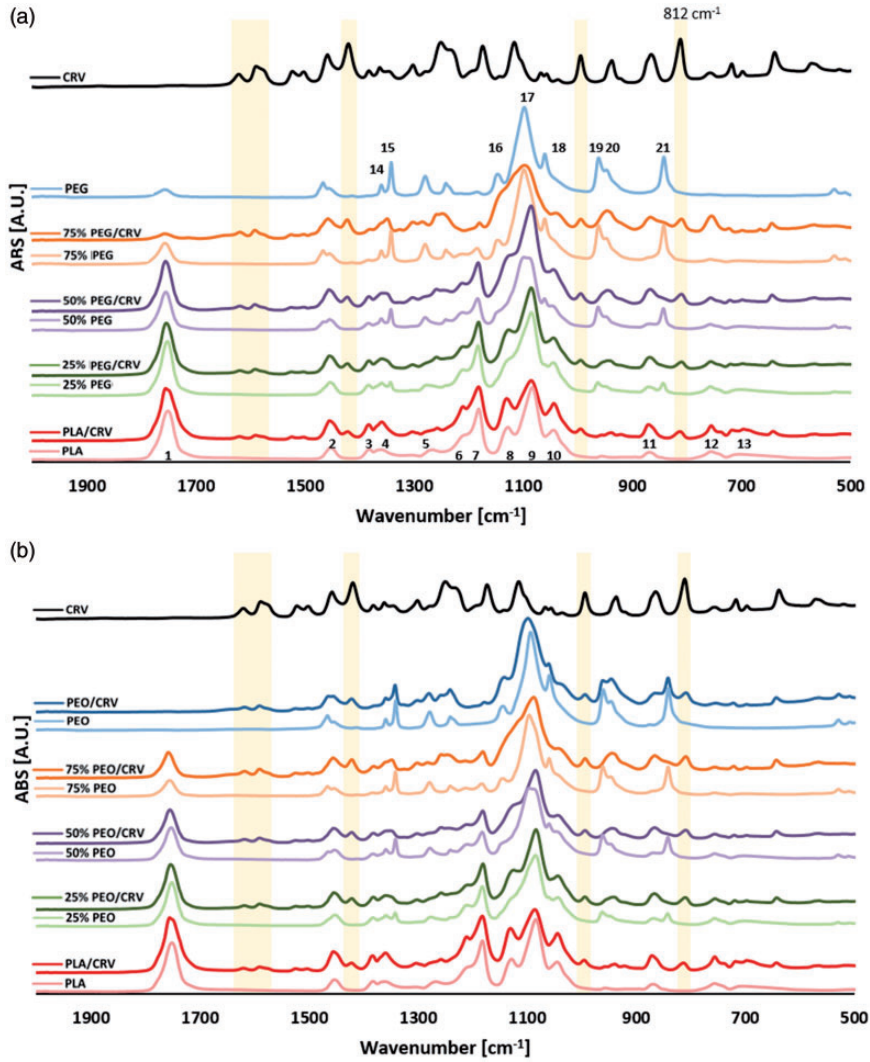

Figure 5. FTIR-ATR measurements of (a) PLA/PEG and PLA/PEG/CRV electrospun fibers and of (b) PLA/PEO and PLA/PEO/CRV electrospun fibers. CRV: carvacrol; PEG: polyethylene glycol; PEO: polyethylene oxide; PLA: polylactic acid.

electrospun mats depends on several variables such as: (i) matrix composition, (ii) surface chemical functional groups, and (iii) morphology of the fibers. As already observed in previous works, the incorporation of CRV in hydrophobic polymers causes a decrease in the contact angle values [63,64]. As expected, the WCA reduction is even more evident in the presence of PEG and PEO and the value of θ_w remains 0° even in PLA/PEG/CRV mats. The increment of θ_w observed for

Table 2. Band assignment for PLA [60] and PEG and PEO [59].

Band number	Assignment	Wavenumber cm^{-1}	Ref
PLA			[60]
1	–C=O carbonyl stretch	1747	
2	$–CH_3$ bend	1456	
3	–CH– asymmetric; symmetric deformation	1382; 1360	
4	–CH– bend	1315–1300	
5	–C–O– stretch	1265	
6	–C=O bend	1211	
7,8,9	–C–O– stretch	1180, 1129, 1083	
10	–OH bend	1044	
11	$–CH_3$ rocking mode	955, 916	
12	–C–C– stretch crystalline phase	869	
13	Amorphous phase	755	
PEG/PEO			[59]
14	–C–C– strech	1360	
15	$–CH_2$ wagging mode	1344 (sym)	
16,17,18	–C–O– strech	1148, 1113, 1061	
19	$–CH_2$ rocking mode	962 (asym)	
20	–C–O– strech	948 (sym)	
21	$–CH_2$ rocking mode	843 (asym)	

PEG: polyethylene glycol; PEO: polyethylene oxide; PLA: polylactic acid.

PLA/PEO/CRV can be likely ascribed to the morphology changes observed with SEM micrographs (Figure 4). The increment of fibers diameter can induce a reduction of porosity of the mats thus avoiding water droplet absorption of the water droplet during the measurements.

Mechanical properties

Representative stress–strain curves of the electrospun PLA, PEO, PLA/PEG (25% PEG, 50% PEG), and PLA/PEO (25% PEO, 50% PEO and 75% PEO) loaded with 28 wt% of CRV or in the absence of CRV are shown in Figure 6. In Figure 7(a–c) and in Table 3 there are reported elastic modulus (Figure 7(a)), tensile strength (Figure 7(b)) and elongation at break (Figure 7(c)) as a function of PEG or PEO amount.

In the inset of Figure 6 some vibrating points likely due to the low force opposed by the highly porous electrospun mats can be observed [19]. The crosshead speed change caused the cusp points visible at 10% strain in the stress–strain curves.

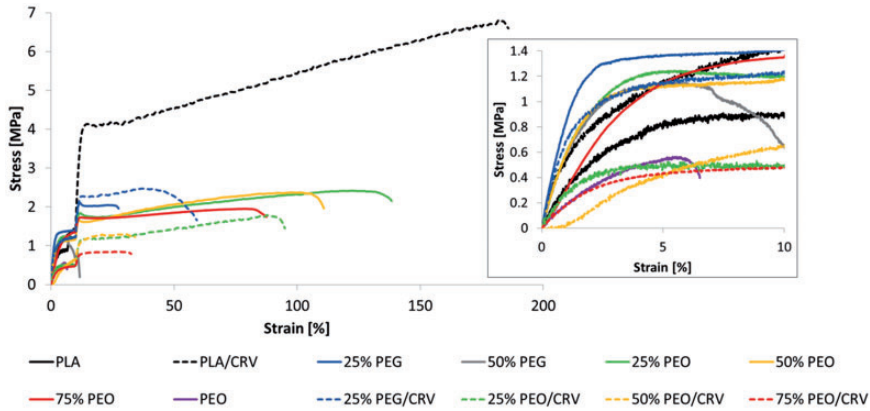

Figure 6. Stress–strain curves of the electrospun membranes loaded with 28 wt% of CRV or in the absence of CRV. CRV: carvacrol; PEG: polyethylene glycol; PEO: polyethylene oxide; PLA: polylactic acid.

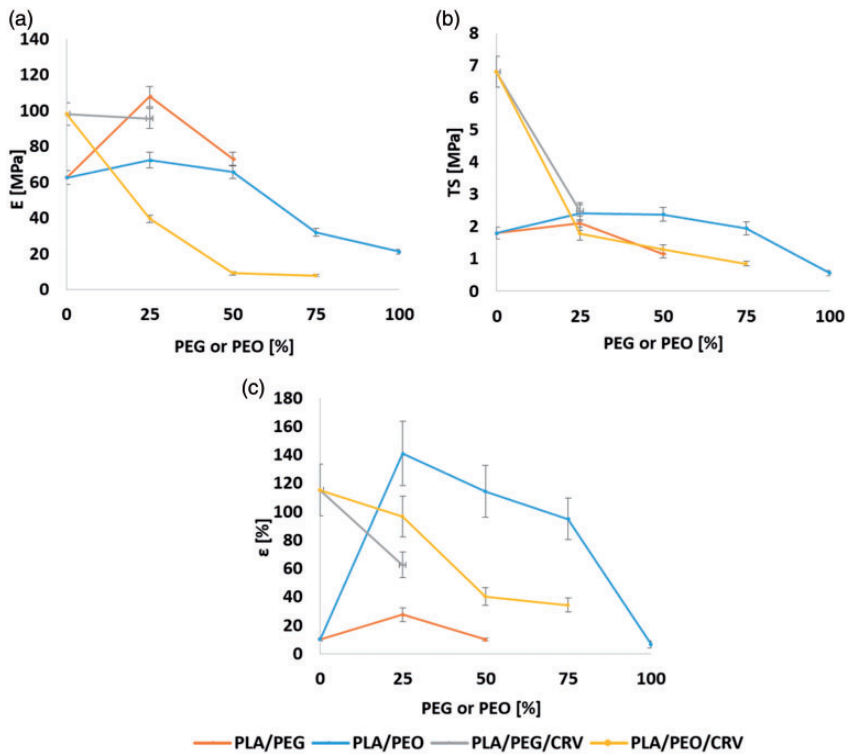

Figure 7. (a) Elastic modulus; (b) tensile strength, and (c) elongation at break of electrospun membranes as a function of PEG or PEO amount loaded with 28 wt% of CRV or in the absence of CRV. CRV: carvacrol; PEG: polyethylene glycol; PEO: polyethylene oxide; PLA: polylactic acid.

Table 3. Elastic modulus (E), tensile strength (TS), and elongation at break (ε) of the electrospun blends.

Sample	E (MPa)	TS (MPa)	ε (%)
PLA	62.50 ± 7.94^{a}	1.80 ± 0.18^{a}	10.17 ± 0.98^{a}
PLA/CRV	98.17 ± 12.30^{b}	6.83 ± 0.49^{b}	113.50 ± 18.43^{b}
25% PEG	107.83 ± 11.69^{b}	$2.13 \pm 0.23^{a,d,e}$	$27.67 \pm 4.63^{a,e}$
50% PEG	73.17 ± 7.52^{a}	1.07 ± 0.12^{c}	10.08 ± 1.02^{a}
25% PEO	72.50 ± 8.96^{a}	2.42 ± 0.21^{d}	141.50 ± 22.62^{c}
50% PEO	65.50 ± 7.26^{a}	$2.33 \pm 0.21^{d,e}$	114.17 ± 18.28^{b}
75% PEO	$31.83 \pm 4.45^{c,d}$	$1.93 \pm 0.22^{a,e}$	94.17 ± 14.29^{b}
PEO	$21.17 \pm 2.48^{c,e}$	5.58 ± 0.08^{f}	6.75 ± 2.52^{a}
25% PEG/CRV	95.50 ± 11.34^{b}	2.47 ± 0.28^{d}	62.33 ± 9.31^{d}
25% PEO/CRV	39.50 ± 3.83^{d}	1.78 ± 0.20^{a}	96.33 ± 14.45^{b}
50% PEO/CRV	$8.97 \pm 1.82^{e,f}$	1.29 ± 0.14^{c}	$40.33 \pm 6.38^{d,e}$
75% PEO/CRV	7.80 ± 1.12^{f}	$0.83 \pm 0.08^{c,f}$	34.17 ± 4.92^{e}

CRV: carvacrol; PEG: polyethylene glycol; PEO: polyethylene oxide; PLA: polylactic acid.
Values are given as means $\pm$ SD. Different letters in the same column indicate significant differences ($p < 0.05$) when analyzed by Tukey's multiple comparisons tests.

The stress–strain curve of PLA electrospun mats presents the typical shape of a brittle material exhibiting a relative high elastic modulus and low elongation at break.

As already observed in some recent works focused on electrospun PLA and PLA/CRV, the presence of CRV can cause an increment of all the investigated mechanical properties [54]. In this work, loading 28 wt% of CRV in PLA causes an increment of the elastic modulus of ~72%; TS increases of ~455%; ε increases of ~1380%.

When compared to PLA, the system loaded with 25 wt% of PEG exhibits an increment of elastic modulus, tensile strength, and elongation of ~72%, ~17%, and ~170%, respectively. The 50% PEG shows a decrease of elastic modulus when compared to 25% PEG but it is still ~17% higher than PLA. For this membrane, the tensile strength is ~36% lower than that of neat PLA while the elongation at break is approximately the same. Electrospun PEO shows the worst mechanical performances with low elastic modulus (~20 MPa), tensile strength (~0.56 MPa), and elongation (~7%).

The mechanical properties of electrospun mats mainly depend not only on the properties of the polymer matrix but also on the additives, on the surface properties, and on the morphological features of the porous structures.

The increment of both elastic modulus and elongation of the electrospun mats containing CRV was already ascribed to the double effect of CRV incorporated in PLA in a previous work [65]. On one hand, CRV can increase the elongation acting as a plasticizer and, at the same time, it can hinder the fibers slipping enhancing the

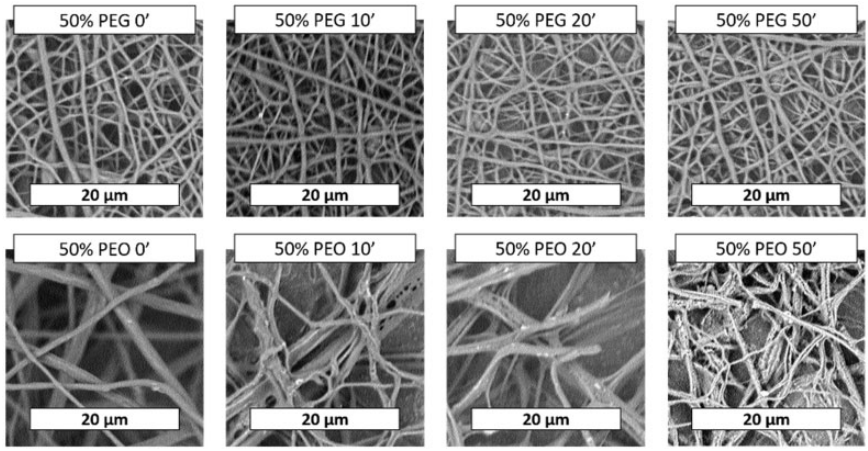

Figure 8. Morphology of the membranes PEG 50 and PEO 50 as a function of the immersion time in distilled water at 80°C. PEG: polyethylene glycol; PEO: polyethylene oxide.

surface interactions between the fibers thus leading to an improvement of the elastic modulus [63,65].

A similar explanation can be assumed for the improved mechanical behavior of blends containing 25 wt% of PEG or PEO. In fact, PEG or PEO can enhance the surface interactions among the fibers and it can increase the mechanical performances of the mats. PEG shows higher reinforcing effect while PEO exhibits higher plasticizer effect.

Neat PEG or PEO displays low values of elastic modulus, tensile strength, and elongation at break. These features can explain the gradual worsening of the mechanical properties of the blends upon increasing PEG or PEO amount.

These results can be likely related to the separation of PEG or PEO from PLA at the solid state. In fact, it is well known that PEG and PEO are partially miscible in PLA and that their miscibility decrease upon increasing the molecular weight [47,48]. In order to observe the eventual phase separation of PEG or PEO from the electrospun fibers, the systems containing 50 wt% of PEG and PEO were immersed in distilled water at 80°C up to 50 min. The temperature was chosen in order to accelerate the separation.

The morphology of the PEG-containing membranes, Figure 8, remains almost constant even after 50 min of immersion thus suggesting that, for this composition, the PEG does not significantly separate from PLA. On the other hand, 50% PEO electrospun mats show an evident change of the fiber's morphology after 10 min of immersion. The finest fibers appear bent while the presence of nanopores on the surface of the largest fibers can be observed. Furthermore, the number of nanopores increases upon increasing the immersion time. This phenomenon can be likely due to the selective leaching of PEO separated from PLA. The different behavior of PEG and PEO can be explained to the difference of their molecular

weight. In particular, PEG (10,000 Da) is probably characterized by higher miscibility in PLA when compared to PEO (100,000 Da) and for this reason any leaching of PEG phase cannot be found. This result, in agreement with other scientific works [66], was already explained taking into account that PEG offers a lower steric encumbrance if compared to PEO and, as a consequence, it better fits among PLA molecular chains: this makes difficult the solid-state phase separation. On the contrary, PEO, which shows a chain length comparable to that of PLA used in this work, tends to re-aggregate at the solid state, thus forming regions with higher concentration that can then be solvated by water [66].

Therefore, the worsening of the mechanical behavior of PLA/PEO blends can be also related to the separation of PEO phase from PLA at the solid state that can act as a defect. This phenomenon is less evident in the PLA/PEG systems that, in fact, exhibit higher elastic modulus in comparison with PLA/PEO blends.

If compared to the corresponding binary blend, the ternary systems show an evident drop of all the mechanical properties on increasing PEG or PEO amount. This behavior can be likely related to the worsening of the fiber morphology induced by the presence of CRV (Figure 4) as already discussed in the previous section.

Release kinetics

The release of CRV is expressed in Figure 9(a,b) as the ratio M_t/M_∞ where M_t is the amount of oil components released at time t, and M_∞ is the theoretical amount of CRV incorporated in the mats. For all the investigated systems, the release of CRV is characterized by three phases. A burst phase in the initial part of the release, a second phase characterized by slower release rate, and a final plateau region, also according to our previous works [54,65].

The results show that all the mats immersed in PBS at 37°C released more than 60% of the whole cumulative oil after 50 h. Furthermore, the levelling off to the plateau region is achieved after 4 to 98 h depending on the blend composition.

In order to understand the release mechanism of the two systems, the experimental data are reported by plotting M_t/M_∞ versus time in logarithmic axes (Figure 9(b)) and fitted using the power law model

$$\frac{M_t}{M_\infty} = kt^n \tag{1}$$

where t is the release time, k is a kinetic constant related to the properties of the drug delivery system, and n is the diffusion exponent that characterizes the release mechanism. In particular, according to Peppas and Sinclair [67], when n is lower than 0.5 the drug release is diffusion-controlled (Fickian), when n is equal to 1.0 it indicates the swelling-controlled drug release [61,68–71].

Values of n between 0.5 and 1.0 can be regarded as an indicator for the superposition of both phenomena defined as anomalous transport. Generally, this model

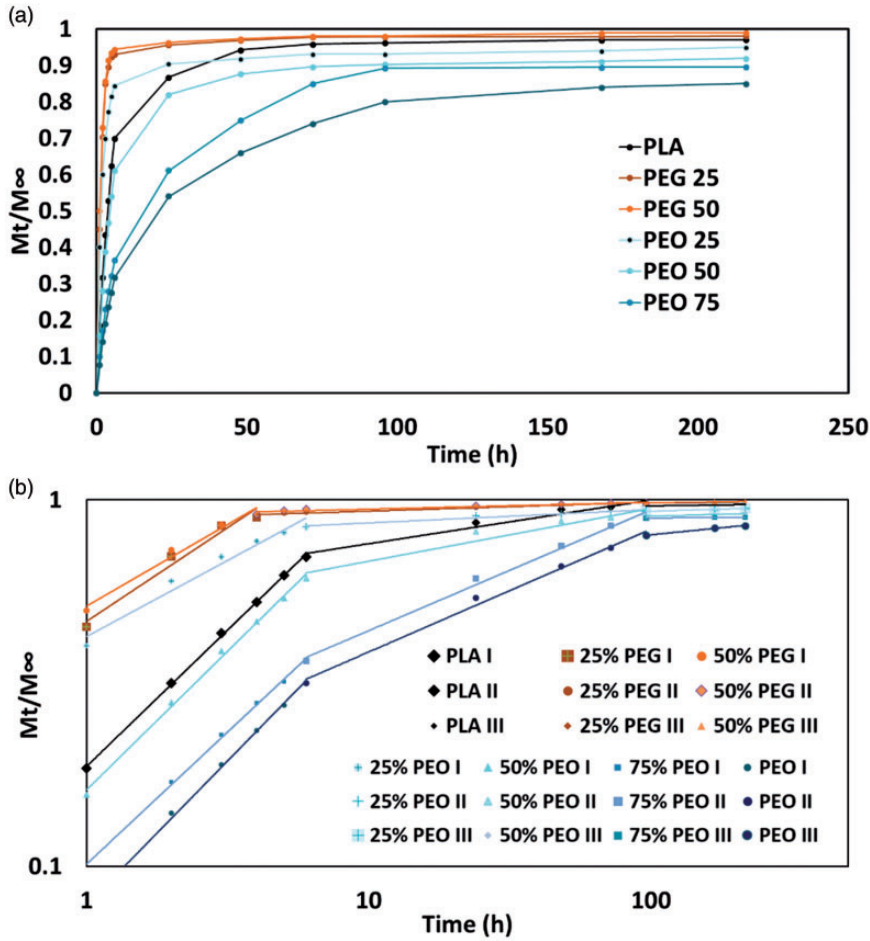

Figure 9. Release kinetics of carvacrol from the electrospun membranes in PBS at 37°C expressed as M_t/M_∞. (a) Linear axes; and (b) logarithmic axes. PEG: polyethylene glycol; PEO: polyethylene oxide; PLA: polylactic acid.

is used to fit the release data in the entire testing time but, according to this rule, the so obtained correlation coefficient (R^2) was not satisfactory. In fact, it is worth nothing that almost all the mathematical models are not able to predict burst effect during drug release. Based on these results, the release data were then fitted by splitting them in three different ranges as reported in another work [58], i.e. the initial burst stage (I), the following slower release rate (II), and the final plateau region (III).

The power law parameters related to the release kinetic of CRV, see Figure 9(b), are listed in Table 4.

Table 4. Power law parameters obtained from the release kinetic of CRV.

	k	*n*	R^2
PLA I	0.1874	0.7452	0.999
25% PEG I	0.4663	0.5123	0.969
50% PEG I	0.514	0.4415	0.976
25% PEO I	0.4238	0.4161	0.967
50% PEO I	0.1618	0.7573	0.996
75% PEO I	0.1014	0.7218	0.998
PEO I	0.0784	0.7878	0.998
PLA II	0.5776	0.1192	0.955
25% PEG II	0.882	0.0241	0.920
50% PEG II	0.9037	0.0189	0.921
25% PEO II	0.7963	0.0363	0.959
50% PEO II	0.4886	0.144	0.930
75% PEO II	0.2062	0.3294	0.993
PEO II	0.178	0.335	0.993
PLA III	0.9128	0.0116	0.959
25% PEG III	0.9683	0.0024	0.954
50% PEG III	0.9253	0.0127	0.955
25% PEO III	0.8384	0.0229	0.933
50% PEO III	0.8177	0.0216	0.931
75% PEO III	0.874	0.0047	0.990
PEO III	0.5641	0.0768	0.985

PEG: polyethylene glycol; PEO: polyethylene oxide; PLA: polylactic acid.

According to these results, it can be hypothesized that PEG promotes CRV release probably increasing PLA chain's mobility and CRV diffusion. The 25% PEO seems to present a similar behavior even if the kinetic is slower upon increasing PEO content. These results can be better explained considering the morphology of the samples after CRV release.

Figure 10 shows the SEM images of the membranes after CRV release in PBS at 37°C. The PEO/CRV morphology is not reported since the membrane in contact with PBS rapidly reduced its apparent volume forming a gelatinous pellet. Both membranes containing PEG show a morphology similar to that before the immersion in PBS. Differently, PEO-containing membranes exhibit a more dense morphology when compared to the pristine ones. In particular, 25% PEO/CRV shows a similar morphology before and after immersion while in 50% PEO/CRV and 75% PEO/CRV the fibers seem to be merged. From these figures, it is possible to assume that the reduced kinetic release of the 50% PEO/CRV and 75% PEO/CRV can be related with the reduced surface area of the membranes due to the change of fiber's

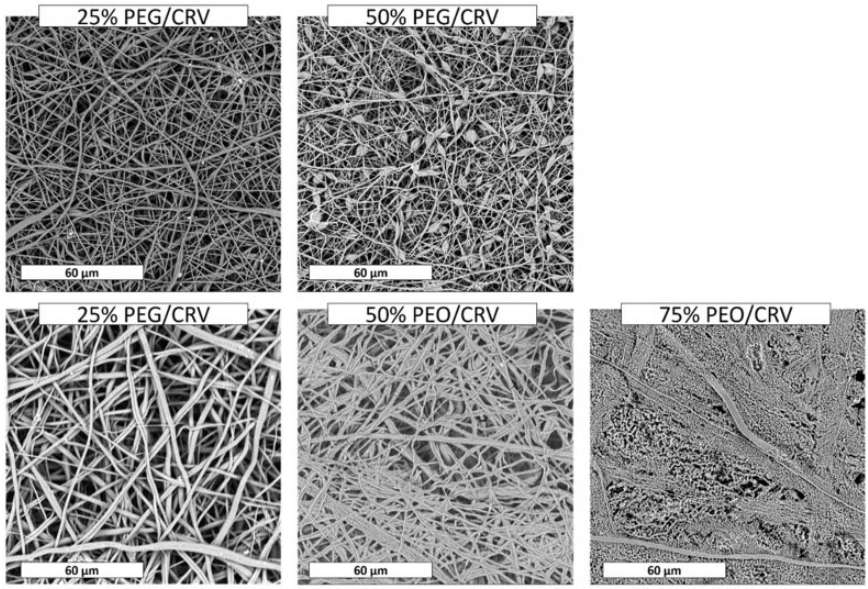

Figure 10. Membranes morphology after 260 h in PBS at 37°C. CRV: carvacrol; PEG: polyethylene glycol; PEO: polyethylene oxide.

morphology. These results suggest that PLA/PEG blends are more suitable for rapid drug release while PLA/PEO blends are preferable for systems needing a more sustainable release.

Conclusions

In this work, a systematic study of PLA/PEG and PLA/PEO electrospun blends at different concentrations was carried out. From a morphological point of view, the fiber's diameter decreased upon increasing the amount of PEG showing beads that become very numerous for 75% PEG mats while neat PEG cannot be electrospun with the chosen processing parameters. PEO induced an enlargement of the fibers diameter and an increase of irregularities of their topology. These results were related with solutions viscosity since, usually, the highest the solution viscosity the highest the fiber's diameter. Accordingly, solution viscosity decreased upon increasing PEG content and increased upon increasing PEO ratio in the blend. The presence of 25% of PEO induced a slight increase of fiber's diameter when compared to neat electrospun PLA. The 50% PEO morphology was found to be very similar to that of PLA while 75% PEO showed very irregular fibers. SEM investigation revealed that neat PEO can be electrospun with the chosen process parameters exhibiting a quite regular fibers morphology. The morphology of CRV-containing membranes is very different from the corresponding blends, in particular for the PLA/PEO systems. The mechanical performances were found to be

improved for blends at low PEG or PEO content, but they worsened in the other cases. PLA added with CRV exhibited higher mechanical properties but they rapidly decreased upon increasing the amount of PEG or PEO. The study of release mechanism through the exponential model highlighted that PEO-containing membranes changed the release mechanism from anomalous drug diffusion in the first 6 h to a Fickian diffusion mechanism for the rest of the test. PEG-containing blends showed, instead, a Fickian diffusion mechanism during the entire release time. Furthermore, from this study it was possible to conclude that the PEG accelerated the kinetic release of CRV while PEO reduced it. This phenomenon was related to the change of morphology during the release from PLA/PEO systems. These results suggested that PEG can be considered a PLA additive suitable for rapid drug release while PEO is preferable for systems needing a more sustainable release.

Declaration of conflicting interests

The author(s) declared no potential conflicts of interest with respect to the research, authorship, and/or publication of this article.

Funding

The author(s) received no financial support for the research, authorship, and/or publication of this article.

ORCID iD

Roberto Scaffaro http://orcid.org/0000-0002-4830-0374

References

[1] Hu X, Liu S, Zhou G, et al. Electrospinning of polymeric nanofibers for drug delivery applications. *J Control Release* 2014; 185: 12–21.
[2] Scaffaro R, Lopresti F, Maio A, et al. Electrospun PCL/GO-g-PEG structures: processing–morphology–properties relationships. *Compos Part A Appl Sci Manuf* 2017; 92: 97–107.
[3] Scaffaro R, Maio A, Lopresti F, et al. Nanocarbons in electrospun polymeric nanomats for tissue engineering: a review. *Polymers* 2017; 9: 76.
[4] Koushki P, Bahrami SH and Ranjbar-Mohammadi M. Coaxial nanofibers from poly(-caprolactone)/poly(vinyl alcohol)/Thyme and their antibacterial properties. *J Ind Text* 2018; 47: 834–852.
[5] Enis IY, Sezgin H and Sadikoglu TG. Full factorial experimental design for mechanical properties of electrospun vascular grafts. *J Ind Text* 2018; 47: 1378–1391.
[6] Song J, Gao H, Zhu G, et al. The preparation and characterization of polycaprolactone/graphene oxide biocomposite nanofiber scaffolds and their application for directing cell behaviors. *Carbon N Y* 2015; 95: 1039–1050.
[7] Azarniya A, Eslahi N, Mahmoudi N, et al. Composites: part A – effect of graphene oxide nanosheets on the physico-mechanical properties of chitosan/bacterial cellulose nanofibrous composites. *Compos Part A* 2016; 85: 113–122.

[8] Zhang Z, Zhang F, Jiang X, et al. Electrospinning and microwave absorption of polyaniline/polyacrylonitrile/multiwalled carbon nanotubes nanocomposite fibers. *Fibers Polym* 2014; 15: 2290–2296.
[9] Zhang L, Yu W, Han C, et al. Large scaled synthesis of heterostructured electrospun TiO_2/SnO_2 nanofibers with an enhanced photocatalytic activity. *J Electrochem Soc* 2017; 164: H651–H656.
[10] Zhang L, Qin M, Yu W, et al. Heterostructured TiO_2/WO_3 nanocomposites for photocatalytic degradation of toluene under visible light. *J Electrochem Soc* 2017; 164: H1086–H1090.
[11] Huang J, Cao Y, Shao Q, et al. Magnetic nanocarbon adsorbents with enhanced hexavalent chromium removal: morphology dependence of fibrillar vs particulate structures. *Ind Eng Chem Res* 2017; 56: 10689–10701.
[12] Li Y, Zhou B, Zheng G, et al. Continuously prepared highly conductive and stretchable SWNT/MWNT synergistically composited electrospun thermoplastic polyurethane yarns for wearable sensing. *J Mater Chem C* 2018; 6: 2258–2269.
[13] Yalcin Enis I and Gok Sadikoglu T. Design parameters for electrospun biodegradable vascular grafts. *J Ind Text* 2018; 47: 2205–2227.
[14] Scaffaro R, Maio A, Lopresti F, et al. Nanocarbons in electrospun polymeric nanomats for tissue engineering: a review. *Polymers* 2017; 9: 1–35.
[15] Gorji M, Karimi M and Nasheroahkam S. Electrospun PU/P(AMPS-GO) nanofibrous membrane with dual-mode hydrophobic–hydrophilic properties for protective clothing applications. *J Ind Text* 2018; 47: 1166–1184.
[16] Scaffaro R, Lopresti F, Sutera A, et al. Plasma modified PLA electrospun membranes for actinorhodin production intensification in *Streptomyces coelicolor* A3(2) immobilized-cell cultivations. *Colloids Surfaces B Biointerfaces* 2017; 157: 233–241.
[17] Goffin AL, Habibi Y, Raquez JM, et al. Polyester-grafted cellulose nanowhiskers: a new approach for tuning the microstructure of immiscible polyester blends. *ACS Appl Mater Interfaces* 2012; 4: 3364–3371.
[18] Navarro-Baena I, Sessini V, Dominici F, et al. Design of biodegradable blends based on PLA and PCL: from morphological, thermal and mechanical studies to shape memory behavior. *Polym Degrad Stab* 2016; 132: 97–108.
[19] Scaffaro R, Lopresti F and Botta L. Preparation, characterization and hydrolytic degradation of PLA/PCL co-mingled nanofibrous mats prepared via dual-jet electrospinning. *Eur Polym J* 2017; 96: 266–277.
[20] Spasova M, Stoilova O, Manolova N, et al. Preparation of PLLA/PEG nanofibers by electrospinning and potential applications. *J Bioact Compat Polym* 2007; 22: 62–76.
[21] Wang BY, Fu SZ, Ni PY, et al. Electrospun polylactide/poly(ethylene glycol) hybrid fibrous scaffolds for tissue engineering. *J Biomed Mater Res Part A* 2012; 100A: 441–449.
[22] Bhattacharjee P, Naskar D, Kim H-W, et al. Non-mulberry silk fibroin grafted PCL nanofibrous scaffold: promising ECM for bone tissue engineering. *Eur Polym J* 2015; 71: 490–509.
[23] Liu Y, Lu J, Xu G, et al. Tuning the conductivity and inner structure of electrospun fibers to promote cardiomyocyte elongation and synchronous beating. *Mater Sci Eng C* 2016; 69: 865–874.
[24] Mukundan S, Sant V, Goenka S, et al. Nanofibrous composite scaffolds of poly(ester amides) with tunable physicochemical and degradation properties. *Eur Polym J* 2015; 68: 21–35.

[25] Thakkar S and Misra M. Electrospun polymeric nanofibers: new horizons in drug delivery. *Eur J Pharm Sci* 2017; 107: 148–167.
[26] Fernandes JG, Correia DM, Botelho G, et al. PHB-PEO electrospun fiber membranes containing chlorhexidine for drug delivery applications. *Polym Test* 2014; 34: 64–71.
[27] Wen P, Zhu D-H, Wu H, et al. Encapsulation of cinnamon essential oil in electrospun nanofibrous film for active food packaging. *Food Control* 2016; 59: 366–376.
[28] Qi YY, Tai ZX, Sun DF, et al. Fabrication and characterization of poly(vinyl alcohol)/graphene oxide nanofibrous biocomposite scaffolds. *J Appl Polym Sci* 2013; 127: 1885–1894.
[29] Zhou H, Lawrence JG and Bhaduri SB. Fabrication aspects of PLA-CaP/PLGA-CaP composites for orthopedic applications: a review. *Acta Biomater* 2012; 8: 1999–2016.
[30] Motealleh B, Zahedi P, Rezaeian I, et al. Morphology, drug release, antibacterial, cell proliferation, and histology studies of chamomile-loaded wound dressing mats based on electrospun nanofibrous poly (ε-caprolactone)/polystyrene blends. *J Biomed Mater Res Part B Appl Biomater* 2014; 102: 977–987.
[31] Brown TD, Edin F, Detta N, et al. Melt electrospinning of poly(ε-caprolactone) scaffolds: phenomenological observations associated with collection and direct writing. *Mater Sci Eng C* 2015; 45: 698–708.
[32] Scaffaro R, Lopresti F, Catania V, et al. Polycaprolactone-based scaffold for oil-selective sorption and improvement of bacteria activity for bioremediation of polluted water: porous PCL system obtained by leaching melt mixed PCL/PEG/NaCl composites: oil uptake performance and bioremediation effi. *Eur Polym J* 2017; 91: 260–273.
[33] Wen P, Zhu D-H, Feng K, et al. Fabrication of electrospun polylactic acid nanofilm incorporating cinnamon essential oil/β-cyclodextrin inclusion complex for antimicrobial packaging. *Food Chem* 2016; 196: 996–1004.
[34] Zhang K, Li G-H, Feng L-M, et al. Ultralow percolation threshold and enhanced electromagnetic interference shielding in poly (l-lactide)/multi-walled carbon nanotube nanocomposites with electrically conductive segregated networks. *J Mater Chem C* 2017; 5: 9359–9369.
[35] Zhao J, Wu L, Zhan C, et al. Overview of polymer nanocomposites: computer simulation understanding of physical properties. *Polymer* 2017; 133: 272–287.
[36] Hutmacher DW. Scaffolds in tissue engineering bone and cartilage. *Biomaterials* 2000; 21: 2529–2543.
[37] Buzarovska A, Gualandi C, Parrilli A, et al. Effect of TiO2 nanoparticle loading on poly(l-lactic acid) porous scaffolds fabricated by TIPS. *Compos Part B Eng* 2015; 81: 189–195.
[38] Scaffaro R, Botta L, Lopresti F, et al. Polysaccharide nanocrystals as fillers for PLA based nanocomposites. *Cellulose* 2017; 24: 447–478.
[39] Scaffaro R, Lopresti F, Botta L, et al. Integration of PCL and PLA in a monolithic porous scaffold for interface tissue engineering. *J Mech Behav Biomed Mater* 2016; 63: 303–313.
[40] Scaffaro R, Sutera F and Lopresti F. Using Taguchi method for the optimization of processing variables to prepare porous scaffolds by combined melt mixing/particulate leaching. *Mater Des* 2017; 131: 334–342.
[41] Thakur VK, Thakur MK, Raghavan P, et al. Progress in green polymer composites from lignin for multifunctional applications: a review. *ACS Sustain Chem Eng* 2014; 2: 1072–1092.

[42] Thakur VK, Singha AS and Thakur MK. Ecofriendly biocomposites from natural fibers: mechanical and weathering study. *Int J Polym Anal Charact* 2013; 18: 64–72.
[43] Wang X, Liu X, Yuan H, et al. Non-covalently functionalized graphene strengthened poly(vinyl alcohol). *Mater Des* 2018; 139: 372–379.
[44] Scaffaro R, Lopresti F, Botta L, et al. A facile and eco-friendly route to fabricate poly(lactic acid) scaffolds with graded pore size. *J Vis Exp* 2016; 116: 1–8.
[45] Scaffaro R, Lopresti F, Botta L, et al. Preparation of three-layered porous PLA/PEG scaffold: relationship between morphology, mechanical behavior and cell permeability. *J Mech Behav Biomed Mater* 2016; 54: 8–20.
[46] Kuang G, Zhang Z, Liu S, et al. Biphasic drug release from electrospun polyblend nanofibers for optimized local cancer treatment. *Biomater Sci* 2018; 6: 324–331.
[47] Huang YY, Chung TW and Tzeng TW. A method using biodegradable polylactides/polyethylene glycol for drug release with reduced initial burst. *Int J Pharm* 1999; 182: 93–100.
[48] Sheth M, Kumar RA, Dave V, et al. Biodegradable polymer blends of poly(lactic acid) and poly(ethylene glycol). *J Appl Polym Sci* 1997; 66: 1495–1505.
[49] Scaffaro R, Lopresti F, Maio A, et al. Electrospun PCL/GO-g-PEG structures: processing-morphology-properties relationships. *Compos Part A Appl Sci Manuf* 2017; 92: 97–107.
[50] Chen J, Liu Z, Chen M, et al. Electrospun gelatin fibers with a multiple release of antibiotics accelerate dermal regeneration in infected deep burns. *Macromol Biosci* 2016; 16: 1368–1380. DOI: 10.1002/mabi.201600108.
[51] Schkarpetkin D, Reise M, Wyrwa R, et al. Development of novel electrospun dual-drug fiber mats loaded with a combination of ampicillin and metronidazole. *Dent Mater* 2016; 32: 951–960.
[52] Zhang Q, Li Y, Lin ZY (William), et al. Electrospun polymeric micro/nanofibrous scaffolds for long-term drug release and their biomedical applications. *Drug Discov Today* 2017; 22: 1351–1366.
[53] Sirc J, Hampejsova Z, Trnovska J, et al. Cyclosporine a loaded electrospun poly(D,L-lactic acid)/poly(ethylene glycol) nanofibers: drug carriers utilizable in local immunosuppression. *Pharm Res* 2017; 34: 1391–1401.
[54] Scaffaro R, Lopresti F, D'Arrigo M, et al. Efficacy of poly(lactic acid)/carvacrol electrospun membranes against *Staphylococcus aureus* and *Candida albicans* in single and mixed cultures. *Appl Microbiol Biotechnol* 2018; 102: 4171–4181.
[55] Scaffaro R, Lopresti F, Marino A, et al. Antimicrobial additives for poly(lactic acid) materials and their applications: current state and perspectives. *Appl Microbiol Biotechnol* 2018; 102: 7739–7756.
[56] Gorrasi G and Pantani R. Effect of PLA grades and morphologies on hydrolytic degradation at composting temperature: assessment of structural modification and kinetic parameters. *Polym Degrad Stab* 2013; 98: 1006–1014.
[57] Wendorff JH, Agarwal S and Greiner A. Electrospinning – some technical aspects. In: *Electrospinning*: Materials, Processing, and Applications. Weinheim, Germany: Wiley-VCH Verlag GmbH & Co., pp.127–142.
[58] Zhou C, Shi Q, Guo W, et al. Electrospun bio-nanocomposite scaffolds for bone tissue engineering by cellulose nanocrystals reinforcing maleic anhydride grafted PLA. *ACS Appl Mater Interfaces* 2013; 5: 3847–3854.
[59] Zhu S, Chen J, Li H, et al. Structure and conformation of poly(ethylene glycol) in confined space of montmorillonite. *Appl Surf Sci* 2013; 264: 500–506.

[60] Scaffaro R, Lopresti F, Botta L, et al. Mechanical behavior of polylactic acid/polycaprolactone porous layered functional composites. *Compos Part B Eng* 2016; 98: 70–77.
[61] Keawchaoon L and Yoksan R. Preparation, characterization and in vitro release study of carvacrol-loaded chitosan nanoparticles. *Colloids Surfaces B Biointerfaces* 2011; 84: 163–171.
[62] Scaffaro R, Lopresti F, Sutera A, et al. Plasma modified PLA electrospun membranes for actinorhodin production intensification in *Streptomyces coelicolor* immobilized-cell cultivations. *Colloids Surfaces B Biointerfaces* 2017; 157: 233–241.
[63] Nostro A, Scaffaro R, D'Arrigo M, et al. Study on carvacrol and cinnamaldehyde polymeric films: mechanical properties, release kinetics and antibacterial and antibiofilm activities. *Appl Microbiol Biotechnol* 2012; 96: 1029–1038.
[64] Nostro A, Scaffaro R, D'Arrigo M, et al. Development and characterization of essential oil component-based polymer films: a potential approach to reduce bacterial biofilm. *Appl Microbiol Biotechnol* 2013; 97: 9515–9523.
[65] Scaffaro R and Lopresti F. Processing, structure, property relationships and release kinetics of electrospun PLA/Carvacrol membranes. *Eur Polym J* 2018; 100C: 165–171.
[66] Scaffaro R, Lo Re G, Rigogliuso S, et al. 3D polylactide-based scaffolds for studying human hepatocarcinoma processes in vitro. *Sci Technol Adv Mater* 2012; 13: 045003.
[67] Peppas NA and Sinclair JL. Anomalous transport of penetrants in glassy polymers. *Colloid Polym Sci* 1983; 261: 404–408.
[68] Scaffaro R, Botta L, Maio A, et al. Effect of graphene nanoplatelets on the physical and antimicrobial properties of biopolymer-based nanocomposites. *Materials* 2016; 9: 351.
[69] Saha NR, Sarkar G, Roy I, et al. Studies on methylcellulose/pectin/montmorillonite nanocomposite films and their application possibilities. *Carbohydr Polym* 2016; 136: 1218–1227.
[70] Ritger PL and Peppas NA. A simple equation for description of solute release II. Fickian and anomalous release from swellable devices. *J Control Release* 1987; 5: 37–42.
[71] Scaffaro R, Botta L, Maio A, et al. PLA graphene nanoplatelets nanocomposites: physical properties and release kinetics of an antimicrobial agent. *Compos Part B Eng* 2017; 109: 138–146.